ACS OMEGA

http://pubs.acs.org/journal/acsodf

Article

Preparation of Micron-Sized TS-1 Spherical Membrane Catalysts and Their Performance in the Epoxidation of Chloropropene

Guoqiang Tang, Yichuan Li,* Zhaosheng Yang, Yu Wang, Guangyun Li, Yilou Wang, Yong-Ming Chai, and Chenguang Liu

Cite This: *ACS Omega* 2023, 8, 19099−19108

Read Online

ACCESS | Metrics & More | Article Recommendations

ABSTRACT: Titanium silica (TS-1) membrane catalysts grown on the surfaces of spherical substrates can both exploit the high catalytic performance and facilitate their separation from products after the reaction. In this work, a simple static crystallization method was used to perform the in situ construction of a TS-1 membrane on the surfaces of micron-sized spherical carriers. The shortcomings of the TS-1 membrane under static crystallization conditions were overcome by in situ dynamic crystallization, and the effect of rotation speed on the formation of the molecular sieve membrane was investigated. The results showed that the molecular sieve membrane was smooth and homogeneous, with a higher synthesis efficiency at a slow rotational speed. The micron TS-1 spherical membrane catalytic chloropropene epoxidation reaction was investigated in a fixed bed, and the conversion of hydrogen peroxide and selectivity of epichlorohydrin reached 99.4 and 96.8%, respectively. After being reused twice, the catalyst still maintained a stable catalytic performance.

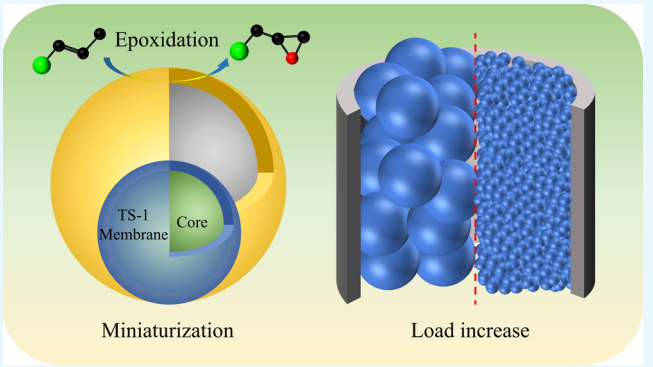

1. INTRODUCTION

Epichlorohydrin (ECH) is an important raw chemical material and organic intermediate that has been widely used in the production of epoxy resin, glycerol, glycidyl ether, quaternary ammonium salt, and chloro-alcohol rubber.[1−3] At present, the main industrial production methods of epichlorohydrin include the chlorination of propylene at high temperatures, the allyl alcohol method, and the glycerol method.[4,5] Traditional production methods cause serious corrosion to equipment, with most of the byproducts being treated by incineration, and generate a large amount of wastewater, thus making this process fail to meet the requirements necessary to be environmentally friendly.[6,7] Titanium silica (TS-1) molecular sieves have been widely used in olefin epoxidation, the hydroxylation of aromatic rings, oxime of cyclohexanone, and the oxidation of alcohols and saturated hydrocarbons using hydrogen peroxide as an oxidant.[8−11] The process of TS-1/H_2O_2 catalyzing propylene chloride epoxidation to produce epichlorohydrin was shown to achieve high efficiency, environmental friendliness, and economic feasibility, greatly simplifying the process and offering good application prospects.[12−18] In industrial production, such as that for HPPO (hydrogen peroxide-epoxyrine), fixed-bed processes have gradually been developed,[19−21] and most catalysts used in fixed beds need to be shaped.[22,23] The binder used in traditional molding methods will cover the surface of the molecular sieve and active sites, leading to a low utilization rate of the catalyst. This problem can be solved by loading the molecular sieve directly on the support surfaces.

TS-1 membranes grown on the surfaces of inorganic nonmetallic materials can be used for the oxidation of industrial organic molecules.[24] This immobilized molecular sieve membrane has become a breakthrough technology for realizing the coupling of the reaction and separation at the catalyst design level.[25−29] Chen et al. and Wang et al. used TS-1 membranes loaded on mullite and alumina, respectively, for the oxidation of isopropyl alcohol and the one-step reaction of benzene to phenol with good catalytic reactivity.[30,31] In our previous work, we prepared a TS-1 membrane with a high *b*-axis orientation on flat stainless steel via in situ hydrothermal crystallization,[32] and further in situ construction of a highly *b*-axis oriented TS-1 membrane was achieved on the surfaces of 2 mm alumina spherical carriers.[33] The immobilized TS-1

Received: April 13, 2023
Accepted: May 4, 2023
Published: May 15, 2023

https://doi.org/10.1021/acsomega.3c02538
ACS Omega 2023, 8, 19099−19108

spherical membrane catalyst had the characteristics of improved mass transfer and easy recovery of the catalyst, and the conversion of hydrogen peroxide and product selectivity reached 87.4 and 93.2%, respectively, in the fixed-bed chloropropene epoxidation reaction. However, during the assessment of catalytic reaction performance, the alumina carrier occupied the majority of the volume in the catalytic bed due to its large size compared to the loaded molecular sieve membrane layer, and the low loading rate of the active components on the carrier limited further improvement of catalytic activity. Qiu et al.[34] loaded the TS-1 membrane prepared for the catalytic styrene oxide reaction on water-resistant SiO_2 spheres with 3−6 mm particle sizes by increasing crystallization times to increase catalyst loading. However, as the number of crystallizations increased, the density and thickness of the membrane affected the diffusion of the reactants and the nonskeleton titanium species in the membrane grains increased, leading to higher selectivity of nontarget products. Because multiple crystallizations were not effective in improving the catalytic activity of the molecular sieve membranes, an appropriate reduction in the carrier size would be an ideal approach to effectively increase the molecular sieve loading rate. However, miniaturization of the spherical carrier size will bring new challenges in the preparation of molecular sieve membranes.

In a previous study, Aguado et al.[35] found that the static crystallization membrane-forming environment led to the deposition of free nuclei from the precursor solution on top of the carrier. These competed with the nuclei that were already adsorbed on the carrier surface for nutrients in the precursor solution, resulting in slow growth of the membrane layer and even defects in the grown membrane layer. The preparation of molecular sieve membranes on microsphere carrier surfaces with a higher curvature could make the above problems more prominent.[33] Dong et al.[36] successfully synthesized a high-quality silicalite-1 membrane on alumina spheres with porous defects using a dynamic hydrothermal method consisting of crystalline seed coating-pre-crystallization-crystallization membrane formation. The dynamic method was found to improve crystallinity, decrease the particle size, and improve catalytic activity.[37] Li et al.[37] synthesized continuous *b*-axis oriented MFI-type molecular sieve membranes on stainless steel sheet supports using the dynamic hydrothermal method in a rotating oven, and the dynamic crystallization method overcame the negative effect of gravitational settling in the static crystallization process. Compared to the static hydrothermal method, the temperature and concentration differences of the synthesis solution in the dynamic crystallization process were greatly reduced, the synthesis time of the membrane layer was short, and the particle size distribution of the molecular sieve was uniform with good orientation.

In this work, the effect of carrier TS-1 membrane construction was investigated using the in situ static crystallization method. The material and size of the carrier were selected by evaluating its epoxidation performance in a fixed-bed reactor. Then, the dynamic crystallization method was successfully implemented on a micrometer scale carrier, and the issue of nonuniform and uneven membrane layers generated by the static crystallization process was improved. Subsequently, we optimized the preparation conditions for the micron-scale molecular sieve, and a uniform TS-1 membrane was constructed in situ on 400 μm zirconia microsphere carriers by screening the carriers and optimizing the crystallization environment. Furthermore, the performance of the microsphere TS-1 membrane catalyst on the epoxidation of chloropropene was evaluated in a fixed bed, where the advantages of integrated reaction separation of the molecular sieve sphere membrane catalyst were initially demonstrated. The catalyst could be separated and reused efficiently, and its high activity could still be maintained after three cycles. The results from this work offer positive implications for the industrial application of TS-1 catalysts.

2. EXPERIMENTAL SECTION

2.1. Reagents and Ingredients. In this work, we utilized tetraethyl orthosilicate (TEOS, mass fraction 99%, Sinopharm Chemical Reagent Co., Ltd.), tetrabutyl titanate (TBOT, mass fraction 99.5%, Shanghai Aladdin Biochemical Technology Co., Ltd.), tetrapropylammonium hydroxide (TPAOH, mass fraction 40%, Shanghai Aladdin Biochemical Technology Co., Ltd.), isopropyl alcohol (IPA, mass fraction 99.5%, Shanghai Aladdin Biochemical Technology Co., Ltd.), methanol (mass fraction 99.5%, Greagent), anhydrous ethanol (mass fraction 99.7%, Greagent), chloropropene (mass fraction 99%, Adamas), hydrogen peroxide (mass fraction 30%, Sinopharm Chemical Reagent Co., Ltd.), toluene (mass fraction 99.5%, Sinopharm Chemical Reagent Co., Ltd.), and nitric acid (mass fraction 65.0−68.0%, Sinopharm Chemical Reagent Co., Ltd.). The carriers consisted of alumina spheres (700 μm) and zirconia spheres (700 and 400 μm).

2.2. Pretreatment of the Carriers. The carrier pellets were first placed in acetone and ultrasonically cleaned for 10 min, followed by several washes with anhydrous ethanol. Afterward, deionized water was used to clean the ethanol on the surface of the carrier, and the carrier was dried overnight in an oven at 120 °C.

To facilitate the growth of TS-1 grains in the *b*-orientation on the surface of the carrier, the carrier had to be modified according to the following method.[33] First, 3.40 g of TBOT was added to 25 g of ethanol and stirred at room temperature for 1 h. Meanwhile, 25.68 g of ethanol, 0.019 g of nitric acid, and 0.54 g of deionized water were mixed under sufficient stirring for 1 h, and then, the above two solutions were mixed and stirred continuously for 24 h to obtain the TiO_2 sol modified solution. The surface of the washed carrier was modified by the dip-coating method, where the modification process was as follows. First, an appropriate amount of TiO_2 solution was used to submerge the carrier spheres, which were allowed to stand for 3 min. Then, excess liquid was poured off and the modified carrier was allowed to stand at room temperature until it dried. Then, the dried carrier was placed in a muffle furnace with a heating program of 0.5 °C/min and roasted at 450 °C for 4 h. The modification process of the above carrier was repeated three times.

The modification solution was obtained by mixing 5.34 g of methanol with 36.86 g of toluene and then stirring for 30 min. Then, 1.13 g of TBOT was added and continuously stirred for 30 min. Subsequently, the carrier spheres loaded with a TiO_2 oxide layer were placed into the TBOT modification solution for 10 min, removed, and washed repeatedly with anhydrous ethanol until the residual modification solution was cleaned. This was followed by hydrolysis in deionized water for 3 min, and then, the above modification process was repeated three times, followed by drying at 50 °C for 2 h using a vacuum oven.

https://doi.org/10.1021/acsomega.3c02538
ACS Omega 2023, 8, 19099−19108

2.3. Preparation of the TS-1 Molecular Sieve Membrane. The molar composition of the precursor solution was $n(\mathrm{TEOS}):n(\mathrm{TBOT}):n(\mathrm{TPAOH}):n(\mathrm{H_2O})$ = 1:0.025:0.15:40. A certain amount of TPAOH was mixed with deionized water and stirred for 30 min, and then, an appropriate amount of TEOS was continuously added at a rate of 20 mL/h using a microsampler. The TEOS was hydrolyzed by continuous stirring for a certain amount of time until the solution changed from turbid to clear and transparent. After mixing a certain amount of IPA with TBOT and stirring for 1 h, the solution was slowly added into the above-clarified solution using the microsampler at a rate of 5 mL/h. After dropwise addition, the solution was stirred for 1 h. Afterward, the solution was heated to 80 °C until all of the IPA was volatilized and removed, and the volume of the precursor solution before and after alcohol removal was replenished with deionized water to ensure that the volume of the precursor solution remained unchanged.

The TS-1 membrane was prepared on the surface of TiO_2-modified and TBOT-modified microsphere carriers (700 μm alumina and zirconia microspheres, 400 μm zirconia microspheres) using the in situ growth method. The 2 mL spheres were placed in 50 mL of PTFE liner, which was poured with the precursor solution, crystallized at 180 °C for an appropriate amount of time, and then removed. The membrane was repeatedly rinsed to pH = 7 using deionized water, dried overnight in an oven at 80 °C, and then roasted at 550 °C for 6 h in a muffle furnace with a temperature increase rate of 1 °C/min.

2.4. Characterization. The X-ray diffraction (XRD) pattern of the samples was determined using a Rayon polycrystalline powder X-ray diffractometer (Panaco, Netherlands), which was used for phase analysis of the materials to calculate the relative crystallinity of the samples, as well as to obtain the bulk phase structure information of the materials. We used a Cu target Kα radiation source (X-ray wavelength λ = 0.15406 nm), where the tube voltage was 45 kV, the tube current was 40 mA, the sample scanning range was 2θ = 10°−75°, and the scanning rate was 8°/min. The Fourier transform infrared (FT-IR) spectrum of the sample was measured by a NEXUS Nicol Corporation (Germany) Fourier transform infrared spectrometer. This characterization method was used to analyze the framework structure and titanium species content of the TS-1 membrane, where the scanning wave number range was 4000−400 cm^{-1}, the scanning resolution was 4 cm^{-1}, and the scans were run 32 times. In addition, the KBr tablet pressing technology was used for testing. The tested sample (accounting for 3% of the total mass) was fully mixed with the KBr solid and ground into a uniform fine powder tablet for testing. The UV−Visible diffuse reflectance spectrum (UV−Vis) of the sample was obtained by a Shimadzu UV-2700 ultraviolet spectrophotometer, which was used to characterize the species and relative content of titanium species in the TS-1 membrane in the molecular sieve, as well as to analyze the coordination state of titanium species in the sample. The detection wavelength ranged from 200 to 700 nm, and $BaSO_4$ was used as a reference. A LabRAM HR Evolution Raman spectrometer was used to determine the sample UV-Raman spectra, with an excitation wavelength of 325 nm. An S4800 cold field emission scanning electron microscope (SEM) (Hitachi, Japan) was used to obtain SEM photos of the sample, which were used to observe the surface morphology and structure of the membrane and the carrier and to intuitively show the synthesis of the TS-1 membrane.

2.5. Catalytic Reaction Evaluation. Continuous reaction activity evaluation of direct epoxidation of propylene chloride was performed on a 20 mL fixed-bed high-pressure microreactor (the reaction process is shown in Figure 1), where a 1

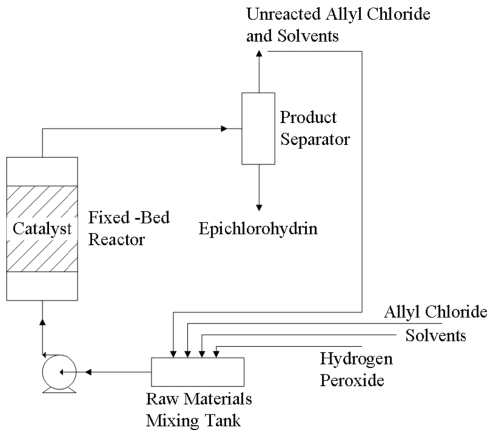

Figure 1. Fixed bed reactor process of the chloropropene epoxidation reaction.

cm-diameter stainless steel reaction tube was filled with a TS-1 membrane catalyst in the middle of the tube and clean quartz sand at both ends of the tube to hold the catalyst in place. During the reaction, nitrogen was continuously pumped into the reaction process to maintain the pressure of the reaction system at 0.5 MPa, and temperature increase rates were set to maintain the temperature of the reaction system at 45 °C. The ratios of reaction materials and reaction conditions were the same as those found in the literature.[33]

2.6. Product Composition Analysis. The concentration of hydrogen peroxide in the reaction and sample mixtures was determined by the indirect iodometric method,[38] where the content of each organic substance in the chloropropene epoxidation reaction products was analyzed by an Agilent 7820A gas chromatograph.

The components of the reaction products were analyzed by the internal standard method, where isobutanol was used as the internal standard. The conversion of hydrogen peroxide ($X_{H_2O_2}$), the selectivity of epichlorohydrin (S_{ECH}), the yield of epichlorohydrin (Y_{ECH}), and the effective utilization of hydrogen peroxide ($U_{H_2O_2}$) were obtained as follows:

$$X_{H_2O_2} = \frac{\omega^0_{H_2O_2} - \omega^i_{H_2O_2}}{\omega^0_{H_2O_2}} \times 100\% \quad (1)$$

$$S_{H_2O_2} = \frac{A_{ECH}}{A_{ECH} + A'} \times 100\% \quad (2)$$

$$Y_{ECH} = \frac{m_{ECH}}{n^0_{H_2O_2} \times M_{ECH}} \times 100\% \quad (3)$$

$$U_{H_2O_2} = \frac{m_{ECH}/M_{ECH}}{m \times (\omega^0_{H_2O_2} - \omega^i_{H_2O_2})} \times 100\% \quad (4)$$

where $\omega^0_{H_2O_2}$ and $\omega^i_{H_2O_2}$ denote the mass fraction of H_2O_2 in the reaction mixture at the beginning and end, respectively; A_{ECH} and A' denote the sum of the chromatographic peak area

https://doi.org/10.1021/acsomega.3c02538
ACS Omega 2023, 8, 19099−19108

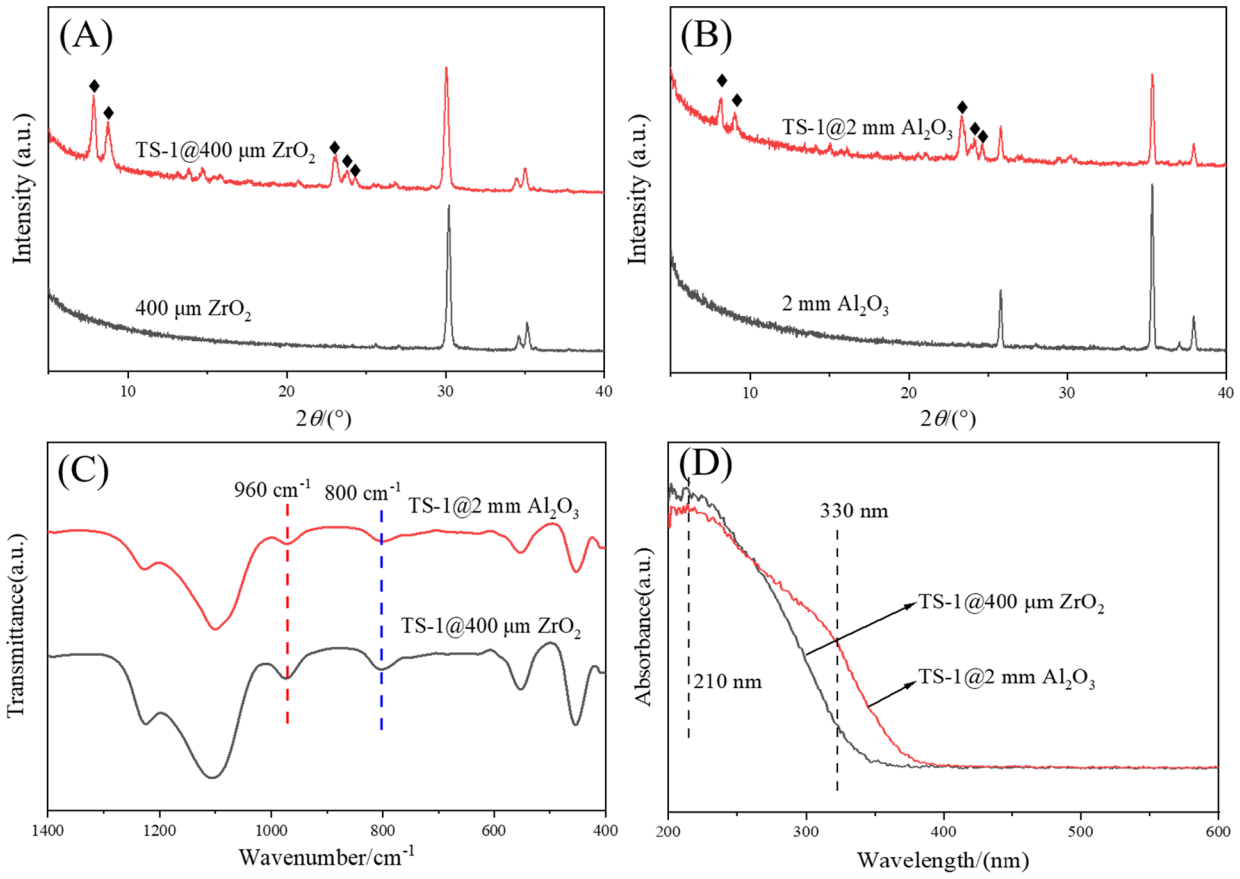

Figure 2. (A) XRD plots of the 2 mm alumina and TS-1 membrane; (B) XRD plots of the zirconia and TS-1 membranes on different sizes of zirconia surfaces; FT-IR plots (C) and UV−vis plots (D) of the TS-1 powders on different carrier kettle bottoms.

of epichlorohydrin and the peak area of the byproducts, respectively, after the reaction; m_{ECH} denotes the total mass of epichlorohydrin in the reaction product and denotes the total mass of the reactants.

3. RESULTS AND DISCUSSION

3.1. Preparation of the Micron-Sized TS-1 Spherical Membrane Catalysts. To achieve miniaturization of the carrier size, 2 mm alumina and 400 μm zirconia microspheres were used as the substrates, and we attempted to grow TS-1 membranes on their surfaces. According to the XRD spectra of the molecular sieve membranes shown in Figure 2A,B, we concluded that the TS-1 membrane was already present on the carrier surfaces when compared with the characteristic XRD peaks of the pure carriers. The characteristic peaks of the MFI topology appeared at 2A = 7.8°, 8.8°, 23.2°, 23.8°, and 24.5°, as shown by the marks in Figure 2A,B. According to the FT-IR spectrum shown in Figure 2C, we found that the intensity of the characteristic peak of 960 cm^{-1} was lower than that of the zirconia support when the substrate consisted of alumina. The characteristic peak at 960 cm^{-1} was likely caused by the asymmetric stretching vibration of the Si−O−Ti bond or the disturbance of the Si−O bond caused by titanium atoms in the framework. This peak generally indicated that titanium atoms entered the framework of the molecular sieve.[39] The UV−vis spectrum depicted in Figure 2D visually shows that the kettle-bottom molecular sieve powder had a more pronounced peak representing anatase at 330 nm when alumina was used as the carrier. The reason for the above phenomenon was possibly because alumina was dissolved in an alkaline crystallization environment to produce Al^{3+}, which inhibited the formation of TS-1 and affected the entry of Ti species into the molecular sieve skeleton, causing the titanium atoms to convert to nonskeleton titanium.[33] In addition, we found that the sample synthesized by miniaturization had a higher peak strength at 210 nm, which indicated that the samples synthesized using zirconia as a support had a higher skeleton titanium content.

Figure 3 shows the SEM images of the TS-1 membrane grown on different carrier sizes and materials under static crystallization conditions. As the size of the spherical carrier continued to decrease, the curvature of the carrier increased, and some of the TS-1 grains on its surface appeared warped. In addition, during the static crystallization process, the membrane layer on the surface of the carrier was not uniform and smooth, with clusters of the molecular sieve on the surface of the membrane layer, where the smaller the size of the carrier, the more the clusters observed. The film layers shown in Figure 3C−F were *b*-oriented; however, the corresponding (0*k*0) peak was not dominant in Figure 2B. The main reasons for this were likely due to the molecular sieve crystals on the zirconia surface, which grew on the curved support and were overlapped and stacked, and due to the distances between the crystal planes being different.[40] Compared to the membrane on the surface of the zirconia carrier, the crystals in the membrane on the alumina surface were elliptical in shape, and the membrane layer that formed was not continuous, with intergranular defects between the molecular sieve particles. The molecular sieve crystals on the zirconia surface were shaped like regular coffins, and the TS-1 grains on the surface

https://doi.org/10.1021/acsomega.3c02538
ACS Omega 2023, 8, 19099−19108

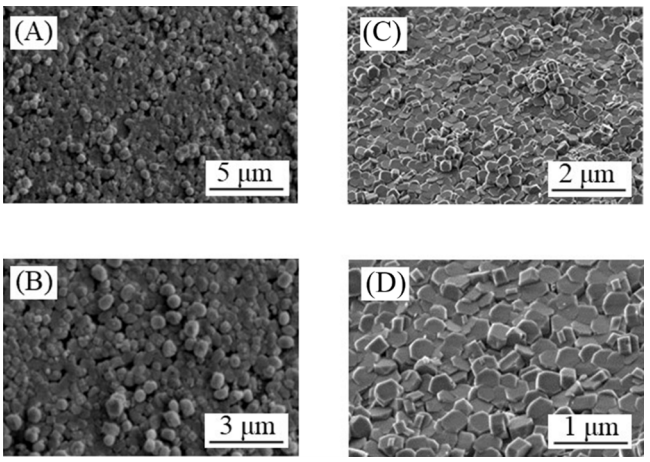

Figure 3. SEM images of the TS-1 membrane on different carrier surfaces under static conditions (A, B for the 2 mm alumina carrier, C, D for the 400 μm zirconia carrier).

of the membrane were well crystallized, forming a continuous membrane. Therefore, zirconia with stronger chemical stability was chosen as the substrate,[41] which was more favorable for the growth of the membrane layer.

The SEM cross-sections of the molecular sieve membranes of different sizes are shown in Figure 4A,B. We found that the molecular sieve membrane thicknesses of the synthesized samples reached 10 and 15 μm, respectively, indicating that miniaturization of the carrier did not cause a loss in thickness of the molecular sieve membrane. In addition, as indicated by the schematic in Figure 4C, carrier miniaturization greatly improved the effective utilization rate of the bed space.

To investigate the mechanical strength of the spherical membrane catalyst, a specific mass of dried spherical membrane catalyst was placed in a beaker containing methanol solution, which was then placed in an ultrasonic cleaning instrument and treated at 45 °C for 2 h. After treatment, the catalyst was dried in an oven at 80 °C. After weighing, we found that the quality of the treated samples did not change significantly, indicating that the prepared spherical membrane catalyst possessed the mechanical strength required for the reaction evaluation process.

3.2. Optimization of the TS-1 Membrane Preparation Process on the Zirconia Microsphere Surface. *3.2.1. Effect of Crystallization Time on the Growth of the Molecular Sieve Membrane.* The effect of crystallization time on the synthesized membrane was observed by the SEM micrographs (crystallization at 180 °C). After 30 h of crystallization, gels and some molecular sieve crystals formed on the surface of the zirconia carrier (Figure 5A,B). After 47 h of crystallization, some disc-shaped crystals formed on the surface of the substrate (Figure 5C,D). After continuing crystallization for 64 h, the TS-1 crystals on the surface of the membrane crystallized into a raspberry-like shape, and some crystals appeared on the surface of the membrane (Figure 5E,F). After 72 h of crystallization, the crystals on the membrane layer continued to grow, and twin crystals appeared on some of the molecular sieve grains; however, the surface of the membrane layer was not attached to the grains, and the membrane layer became smooth and uniform.

To understand the crystallization pattern of the membrane on the surfaces of the zirconia carriers, XRD analysis was performed on the membranes crystallized at different times (Figure 6). After 47 h of dynamic crystallization, there was only one broad peak in the spectrum, indicating that the long-range ordered solid crystals had not yet formed in the solid phase. With increasing crystallization time, sharp characteristic peaks of the MFI structure started to appear in the spectrum, and the peak intensity gradually increased. When the crystallinity of the sample crystallized at 72 h was 100%, the crystallinities of the samples crystallized at different times were calculated by counting the sum of the intensities of the five characteristic peaks, with 2θ values of 7.8°, 8.8°, 23.1°, 23.8°, and 24.2° (Table 1). We found that the crystallinity increased rapidly with prolonged crystallization time after 47 h. The crystallinity reached its maximum after 64 h of crystallization. Because short-range ordered crystals could not be detected by XRD, a molecular sieve membrane possibly started to form at 47 h of crystallization. The diffraction peak intensity of the membrane at 72 h was slightly lower than that of the membrane at 64 h. Table 1 also shows that the relative crystallinity of the membrane at 72 h was also reduced compared to that at 64 h. We found that rotational crystallization improved the crystallization efficiency of the molecular sieve, and there was an issue with excessive crystallization in the dynamic crystallization condition for 72 h.

Figure 7 shows the FT-IR spectra obtained for the resulting powder from the bottom of the kettle at different crystallization times under rotational crystallization conditions. When the crystallization time was 30 h, characteristic absorption peaks at 1226 and 555 cm^{-1} appeared, indicating that the TS-1 molecular sieve membrane with an MFI structure formed when the crystallization time was 30 h.[42,43] The 960 cm^{-1} absorption peak that appeared in the sample after roasting could be used as evidence for the entry of Ti^{4+} into the skeleton.[44] The ratios of relative peak intensities at 960 and 800 cm^{-1} were used to characterize the content of effective Ti^{4+}(different forms of Ti other than anatase) (Table 1), and the I960/I800 value increased with prolonged static crystallization, indicating a higher content of effective Ti^{4+}. In addition, I960/I800 remained at a maximum value at 64 h, indicating the highest amount of skeletal Ti^{4+} content at this

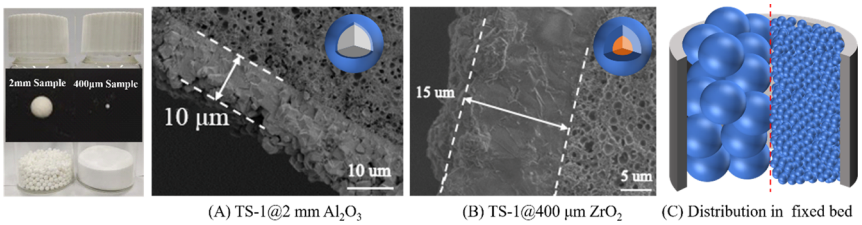

Figure 4. Spherical membrane catalyst cross-section SEM images (A) and (B) and the distribution diagram of spherical membrane catalysts with different sizes in the fixed bed (C).

https://doi.org/10.1021/acsomega.3c02538
ACS Omega 2023, 8, 19099−19108

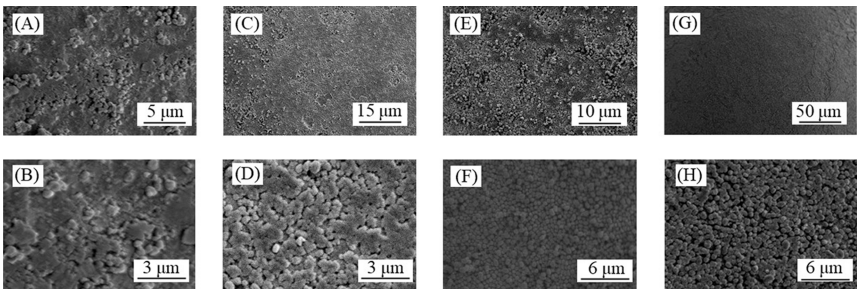

Figure 5. SEM photographs of the TS-1 membrane obtained by the dynamic method at different times (A, B for 30 h of crystallization; C, D for 47 h of crystallization; E, F for 64 h of crystallization; G, H for 72 h of crystallization).

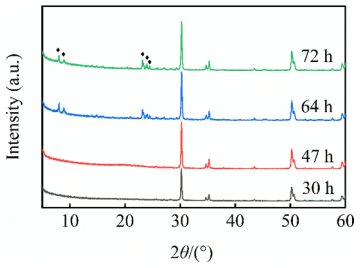

Figure 6. XRD spectrum of the TS-1@ZrO_2 membrane during dynamic crystallization.

Table 1. Relative Crystallinity of the Membrane and I960/I800 Values of the TS-1 Powders at the Bottom of the Kettle after Different Crystallization Times

crystallization time	relative crystallinity	I960/I800
30 h	0.34	0.94
47 h	0.43	0.97
64 h	1.41	0.98
72 h	1	0.83

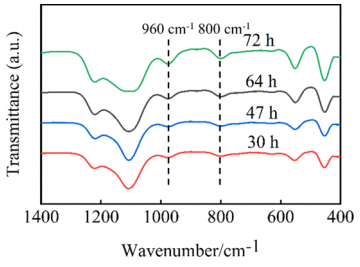

Figure 7. FT-IR spectra of the powders at the bottom of the kettle during dynamic crystallization.

time, where the Ti signal started to decrease beyond 64 h, which was possibly due to the process of holocrystalline substitution of Ti by Si.[45]

During the crystallization process of the TS-1 molecular sieve in the kettle, the presence status of Ti species in the gel affected the entry of Ti atoms into the molecular sieve skeleton. Once TiO_2 crystals formed in the system, it was difficult for the Ti atoms in TiO_2 to enter the molecular sieve skeleton, which led to a decrease in the catalytic activity of the TS-1 molecular sieve. UV−vis spectroscopy is one of the more sensitive methods for characterizing TiO_2 crystals.[46,47] Figure 8A shows the UV−vis spectra of the kettle-bottom powders characterized under different crystallization times under rotational crystallization conditions. When crystallized for 30 h, a peak near 250 nm was observed in the UV−vis spectrum,

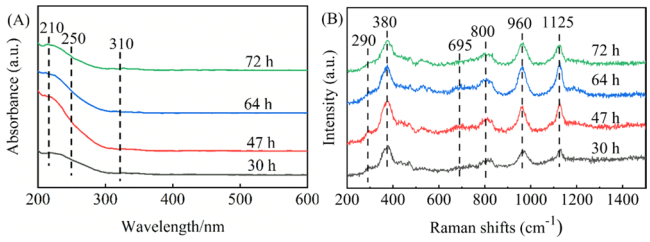

Figure 8. UV−vis (A) and UV-Raman (B) spectra of the powder at the bottom of the kettle during dynamic crystallization.

which consisted of the characteristic absorption peak of the dispersed nonskeletal titanium species TiO_x. When the crystallization time was prolonged, the 250 nm absorption peak was gradually displaced to 210 nm, which was attributed to the characteristic absorption of the skeletal titanium.[46−48] This showed that in the crystallization process of the molecular sieve membrane, Ti entered the skeleton and transformed into tetra-coordinated active Ti species.

UV-Raman spectroscopy is a powerful tool for characterizing the titanium coordination state in TS-1 molecular sieves, as shown in Figure 8B. According to the spectrogram, all samples showed strong peaks at 290, 380, 800, 960, and 1125 cm^{-1} when excited at 325 nm, and the spectral peaks at 290, 380, and 800 cm^{-1} were considered to be the signal peaks of the MFI molecular sieve structure. The characteristic peaks at 960 and 1125 cm^{-1} were the asymmetric stretching and symmetric stretching vibrations of the TiO^4 unit in the molecular sieve framework.[49] The peak at 695 cm^{-1} was caused by stretching vibration of the Ti-O bond in the TiO_6 octahedron.[50] After 30 h of crystallization time, the peak intensity at 695 cm^{-1} gradually decreased, and the skeleton of the titanium content of the sample could be determined by the peak intensity at 1125 cm^{-1}. With extended crystallization time, the peak intensity at 1125 cm^{-1} first increased and then decreased, which indicated that prolonging the crystallization time was conducive to Ti entering the molecular sieve framework. However, extensive crystallization time could lead to loss of the titanium skeleton.

Based on the synthesis of the TS-1 membrane on the surfaces of the zirconia microspheres, as well as by controlling the crystallization time, combined with the heterogeneous nucleation mechanism and the above experimental results,[51] we concluded that during static crystallization, the silicon source was hydrolyzed during aging, forming small gel particles that were deposited on the carrier surface and gradually formed a thin gel layer. During the crystal growth process, the gel was continuously consumed until it came into contact with the carrier surface. At the same time, the nuclei that precipitated

https://doi.org/10.1021/acsomega.3c02538
ACS Omega 2023, 8, 19099−19108

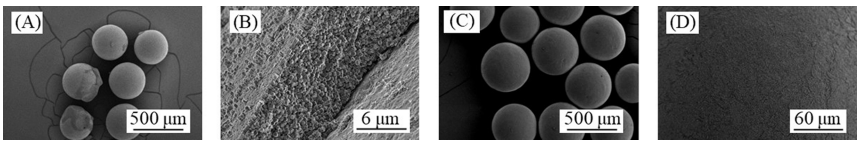

Figure 9. Low-fraction SEM images of the TS-1 membrane synthesized by in situ static (A, B) and dynamic (C, D) methods.

from the mother liquor were preferentially deposited by gravity onto the colloidal layer adsorbed on the surface of the carrier, and the deposited nuclei reduced the rate of nutrients absorbed by the colloidal layer from the mother liquor. Thus, the rate of crystal deposition and growth was greater than the growth rate of the colloidal layer itself.

3.2.2. Effect of Rotating Speed of the Crystallization Kettle on the Growth of the Molecular Sieve Membrane. The defects of the static in situ crystallization method were more easily observed in the low-magnification SEM images. Figure 9A,B shows that during the static crystallization process, numerous molecular sieve crystals accumulated on the carrier surface due to the gravitational settling effect of the TS-1 crystals, with some of the membrane layers exhibiting a thickness of 6 μm. The cross-linking growth of the molecular sieves caused the microsphere carriers to adhere together, resulting in violent breakage that led to discontinuous membrane layers. To overcome the disadvantages of the static crystallization process, a membrane was synthesized by the dynamic crystallization method at a speed of 1 r/min on the surface of the 400-μm zirconia carrier, as shown in Figure 9C,D. The surface of the synthesized membrane was uniform and smooth, with no issues of over-thickness and defects of the membrane layer caused by static crystallization. In addition, the quality of the membrane layer synthesized by dynamic crystallization was superior to the static synthesis process.

Zirconia carriers with a particle size of 400 μm were selected to explore the effect of dynamic rotation speed on the synthesized membrane. Figure 10 shows the SEM images of

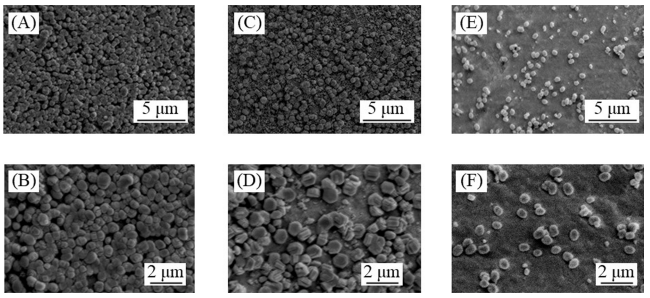

Figure 10. SEM photographs of the synthesized TS-1 membranes at different rotation speeds (A, B at 1 r/min; C, D at 1.5 r/min; E, F at 2.5 r/min).

the membrane synthesized at a rotation speed of 1−2.5 r/min. With increasing dynamic crystallization rotation speed, the grain coverage decreased, the degree of cross-linking decreased, and the exposed area of the substrate gradually increased. The zirconia carrier microspheres increasingly collided with each other in the rotating crystallization kettle at a higher rotational speed and the scouring effect of the fluid also increased, leading to the gradual appearance of defects in the membrane. As shown in Figure 11A, the intensities of the characteristic diffraction peaks of the TS-1 crystals that appeared at 7.96°, 8.87°, 23.20°, 24.10°, and 24.53° for the

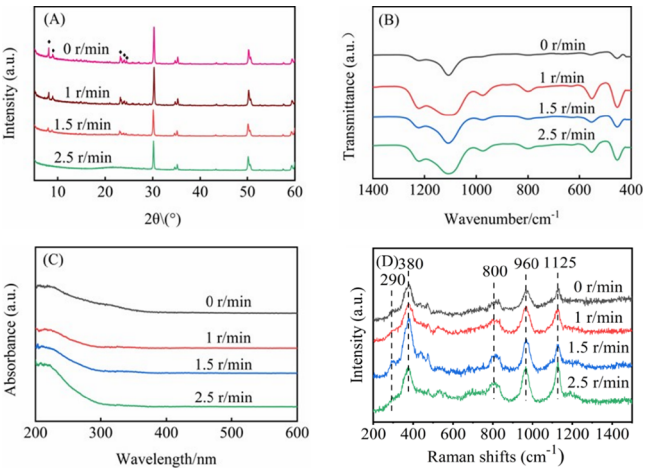

Figure 11. Characterization of the synthetic samples at different rotational speeds: (A) XRD spectra; (B) FT-IR spectra; (C) UV−vis spectra; (D) UV-Raman spectra.

three samples continuously decreased as the rotational speed increased, unlike the static crystallized membrane, which was consistent with the SEM observations.

When the rotation speed of the crystallization kettle was 1 r/min (Figure 10A,B), the carrier surface was dominated by a smooth membrane, and the positions between the TS-1 grains were relatively independent. However, gaps appeared between some of the grains and sporadic twinning appeared. When the crystallization kettle speed was increased to 1.5 r/min (Figure 10C,D), the crystal morphology in the membrane changed significantly, the grain diameter increased, and obvious TS-1 twins appeared. The long crystallization time led to solvent trans-crystallization of the molecular sieve to another more thermodynamically stable X-type molecular sieve. Therefore, the appearance of twin crystals in the membrane was possibly caused by the longer synthesis time.[52] The increase in rotation speed reduced the number of TS-1 crystals adsorbed on the substrate surface, and the nuclei that were deposited on the carrier surface during the synthesis process could fully contact the precursor and absorb more nutrients, which prolonged the crystallization time under high growth efficiency and led to increasingly obvious twinning.[53] When the speed was increased to 2.5 r/min (Figure 9E,F), the membrane could not form. Therefore, the optimal dynamic crystallization speed was 1 r/min. Compared to the membrane generated by static crystallization (Figure 3E,F), at a very slow rotational speed (Figures 9A,B and 10C,D) most of the molecular sieves that adsorbed on the base surface were warped and stacked and were washed or brushed-off and inverted on the carrier surface due to scouring of the precursor solution and friction between the carriers, which facilitated the synthesis of a smooth surface membrane.

Figure 11B shows the FT-IR spectra of the TS-1 powder at the bottom of the kettle at different rotational speeds, where the 4 samples had IR absorption peaks at wave numbers of

https://doi.org/10.1021/acsomega.3c02538
ACS Omega 2023, 8, 19099−19108

Table 2. Reactivity of Different Particle Size Samples for the Catalytic Epoxidation of Chloropropene in a Fixed-Bed Reactor

catalyst	carrier particle size	$X_{H_2O_2}$/%	S_{ECH}/%	Y_{ECH}/%	$U_{H_2O_2}$/%
TS-1@2 mm Al_2O_3	2 mm	89.4	84.2	75.3	89.4
TS-1@400 μm ZrO_2	400 μm	99.4	96.8	92.1	95.7
C-TS-1	20−40 mesh	99.1	92.8	86.0	93.5

450, 550, 800, 1100, and 1225 cm^{-1}. This proved that the synthesized samples exhibited MFI topology, and the samples had obvious absorption peaks near 960 cm^{-1}, indicating that Ti successfully entered the membrane layer of the TS-1 molecular sieve skeleton. The coordination state of Ti in the TS-1 powder in the kettle was analyzed by the UV−vis spectrum, as shown in Figure 11C. Characteristic peaks at 210−220 nm appeared in the spectra, indicating the formation of Ti^{4+} species in all samples. With an increase in rotational speed, the framework Ti^{4+} species content gradually increased. Figure 11D shows the Raman spectra of TS-1 with different titanium contents collected by the 325 nm laser line. The peaks observed at 290, 380, and 800 cm^{-1} were the characteristic peaks of the MFI molecular sieve, while the characteristic peaks at 960 and 1125 cm^{-1} were the asymmetric stretching and symmetric stretching vibrations of the TiO^4 unit in the molecular sieve framework.[49] We could estimate from the peak intensity of the two sites that the skeleton titanium content of the molecular sieve gradually increased with an increase in rotation speed.

With increasing rotational speed, the crystalline nuclei in the mother liquor were evenly dispersed in the flowing crystallization liquid, and the colloidal layer preferentially adsorbed on the surface of the carrier and continuously absorbed the so-called nutrients from the mother liquor. Therefore, they grew and crosslinked, and at this time, the speed of crystallization, growth, and crosslinking in the gel layer and on the surface of the carrier was greater than the speed of particle deposition, and the surface of the membrane became smooth and flat. As the speed continued to increase, the factors that disturbed the growth environment of the membrane on the surface of the carrier increased, preventing the membrane from forming a continuous layer, or even a membrane layer at all.[37]

3.3. Evaluation of the Catalytic Performance of the TS-1 Spherical Membrane in the Fixed Bed. The TS-1 spherical membranes prepared on carriers of different sizes were used as catalysts to investigate the effect of the carrier size on the epoxidation reaction of chloropropene in a fixed bed, and the catalyst evaluation results are shown in Table 2. The powder at the bottom of the kettle of the TS-1@400 μm ZrO_2 sample was extruded and denoted as C-TS-1. Compared to the spherical membrane on the 2 mm carriers, as the loading capacity of the molecular sieve and the utilization rate of the bed improved, nearly 100% conversion of hydrogen peroxide was achieved when the size decreased to 400 μm. The TS-1@400 μm ZrO_2 sample had a higher effective utilization rate of H_2O_2 than the TS-1@2 mm Al_2O_3 sample, which confirmed the phenomenon shown in Figure 2D, where the framework titanium content of the TS-1@400 μm ZrO_2 sample was higher than the TS-1@2 mm Al_2O_3 sample. In addition, compared to the extruded sample, the TS-1@400 μm ZrO_2 sample showed better catalytic performance, possibly because more active sites could be exposed by the spherical membrane catalyst.

The micron spherical support enabled the highly efficient separation and recovery of the immobilized catalyst particles in the fixed bed process. Cycling experiments of the chloropropene epoxidation reaction with spherical membrane catalysts were carried out in a fixed bed at a reaction temperature of 45 °C. The catalyst was recovered by filtration, rinsed three times with methanol, dried at 50 °C, and then put back into use. The reaction results are shown in Table 3. The catalytic activity remained stable after the catalyst was reused twice.

Table 3. Effect of Reuse Frequency on the Epoxidation Performance of Chloropropene

reuse times	S_{ECH}/%	Y_{ECH}/%	$X_{H_2O_2}$/%	$U_{H_2O_2}$/%
0	96.8	92.1	99.4	95.7
1	95.8	91.2	98.4	95.8
2	94.9	90.3	97.4	93.8

4. CONCLUSIONS

The effects of the microsphere carrier material and size as well as the crystallization environment on the growth of the TS-1 membrane were comprehensively investigated by in situ hydrothermal crystallization. The membranes grown on the surfaces of the zirconia carriers were of better quality than those grown on the alumina surfaces, and they were less prone to the formation of nonskeletal Ti. The different curvatures of the spherical carriers with different sizes potentially affected the flatness of TS-1 on the carrier surface, resulting in the stacking of molecular sieve grains. In addition, we found that the dynamic crystallization method effectively avoided grain stacking in the crystallization process during synthesis. Rotational crystallization at a speed of 1 r/min made it easier to synthesize uniform and smooth TS-1 membranes; however, the defects of the TS-1 membrane on the surfaces of the microspheres gradually increased with increasing speed. Micron-sized molecular sieve sphere membrane catalysts with optimized conditions were used to catalyze the epoxidation reaction of chloropropene in a fixed bed, and the conversion rate of hydrogen peroxide was 99.4%, while the selectivity of epichlorohydrin was 96.8% when the reaction temperature was 45 °C. The catalytic performance of the TS-1 molecular sieve spherical membrane catalyst remained steady after two separation and reuse cycles.

■ ASSOCIATED CONTENT

Data Availability Statement

All data generated or analyzed during this study are included in this published article.

■ AUTHOR INFORMATION

Corresponding Author

Yichuan Li − *State Key Laboratory of Heavy Oil Processing, College of Chemical Engineering, China University of Petroleum (East China), Qingdao, Shandong 266580, China;* orcid.org/0000-0003-0615-7706; Phone: +86-

https://doi.org/10.1021/acsomega.3c02538
ACS Omega 2023, 8, 19099−19108

532-86984686; Email: liyichuan@upc.edu.cn; Fax: +86-532-86981787

Authors

Guoqiang Tang − *State Key Laboratory of Heavy Oil Processing, College of Chemical Engineering, China University of Petroleum (East China), Qingdao, Shandong 266580, China;* orcid.org/0000-0002-7126-0171

Zhaosheng Yang − *State Key Laboratory of Heavy Oil Processing, College of Chemical Engineering, China University of Petroleum (East China), Qingdao, Shandong 266580, China*

Yu Wang − *State Key Laboratory of Heavy Oil Processing, College of Chemical Engineering, China University of Petroleum (East China), Qingdao, Shandong 266580, China*

Guangyun Li − *State Key Laboratory of Heavy Oil Processing, College of Chemical Engineering, China University of Petroleum (East China), Qingdao, Shandong 266580, China*

Yilou Wang − *State Key Laboratory of Heavy Oil Processing, College of Chemical Engineering, China University of Petroleum (East China), Qingdao, Shandong 266580, China*

Yong-Ming Chai − *State Key Laboratory of Heavy Oil Processing, College of Chemical Engineering, China University of Petroleum (East China), Qingdao, Shandong 266580, China*

Chenguang Liu − *State Key Laboratory of Heavy Oil Processing, College of Chemical Engineering, China University of Petroleum (East China), Qingdao, Shandong 266580, China*

Complete contact information is available at: https://pubs.acs.org/10.1021/acsomega.3c02538

Author Contributions

G.T.: writing − original draft & editing, methodology, and formal analysis. Y.L.: writing − review & editing, methodology, conceptualization, and funding acquisition. Z.Y.: writing − original draft, data curation, methodology, and formal analysis. Y.W.: writing − original draft and data curation. G.L. and Y.W.: data collection and validation. Y.-M.C.: writing − review & editing and resources. C.L.: writing − review & editing and validation.

Notes

The authors declare no competing financial interest.

■ ACKNOWLEDGMENTS

This work was supported by the Shandong Provincial Natural Science Foundation (No. ZR2022MB090) and the Fundamental Research Funds for the Central Universities (No. 20CX02211A).

■ ABBREVIATIONS

TS-1tabtitanium silica
TPAOHtabtetrapropylammonium hydroxide
TPABrtabtetrapropyl ammonium bromide
SDAtabstructure directing agent
TBOTtabtetrabutylorthotitanate
TEOStabtetraethyl orthosilicate
IPAtabisopropyl alcohol
ACLtaballyl chloride
MeOHtabmethanol
ECHtabepichlorohydrin
TPA^+tabtetrapropylammonium

■ REFERENCES

(1) Wang, M.; Zhou, J.; Mao, G.; Zheng, X. Synthesis of TS-1 from an Inorganic Reactant System and Its Catalytic Properties for Allyl Chloride Epoxidation. *Ind. Eng. Chem. Res.* **2012**, *51*, 12730−12738.
(2) Krzyżanowska, A. M.; Milchert, E.; Październioch, W. M. Technological Parameters of Dehydrochlorination of 1,3-Dichloropropan-2-ol to Epichlorohydrin. *Ind. Eng. Chem. Res.* **2013**, *52*, 10890−10895.
(3) Wang, Q.; Mi, Z.; Wang, Y.; Wang, L. Epoxidation of allyl choride with molecular oxygen and 2-ethyl-anthrahydroquinone catalyzed by TS-1. *J. Mol. Catal. A: Chem.* **2005**, *229*, 71−75.
(4) Almena, A.; Martín, M. Technoeconomic Analysis of the Production of Epichlorohydrin from Glycerol. *Ind. Eng. Chem. Res.* **2016**, *55*, 3226−3238.
(5) Li, J.; Zhao, G.; Gao, S.; Lv, Y.; Li, J.; Xi, Z. Epoxidation of Allyl Chloride to Epichlorohydrin by a Reversible Supported Catalyst with H2O2 under Solvent-Free Conditions. *Org. Process Res. Dev.* **2006**, *10*, 876−880.
(6) Ding, L.; Yin, J.; Tong, W.; Peng, R.; Jiang, J.; Xu, H.; Wu, P. Selective synthesis of epichlorohydrin via liquid-phase allyl chloride epoxidation over a modified Ti-MWW zeolite in a continuous slurry bed reactor. *New J. Chem.* **2021**, *45*, 331−342.
(7) Wang, S.-J.; Wong, D. S.-H.; Lim, I. J. Q.; Chen, Y.-T.; Huang, C.-C. Design and Control of a Novel Plant-Wide Process for Epichlorohydrin Synthesis by Reacting Allyl Chloride with Hydrogen Peroxide. *Ind. Eng. Chem. Res.* **2018**, *57*, 6926−6936.
(8) Wróblewska, A.; Tołpa, J.; Kłosin, D.; Miądlicki, P.; Koren, Z. C.; Michalkiewicz, B. The application of TS-1 materials with different titanium contents as catalysts for the autoxidation of α-pinene. *Microporous Mesoporous Mater.* **2020**, *305*, No. 110384.
(9) Soekiman, C. N.; Miyake, K.; Hayashi, Y.; Zhu, Y.; Ota, M.; Al-Jabri, H.; Inoue, R.; Hirota, Y.; Uchida, Y.; Tanaka, S.; et al. Synthesis of titanium silicalite-1 (TS-1) zeolite with high content of Ti by a dry gel conversion method using amorphous TiO_2−SiO_2 composite with highly dispersed Ti species. *Mater. Today Chem.* **2020**, *16*, No. 100209.
(10) Smeets, V.; Gaigneaux, E. M.; Debecker, D. P. Hierarchical micro−/macroporous TS-1 zeolite epoxidation catalyst prepared by steam assisted crystallization. *Microporous Mesoporous Mater.* **2020**, *293*, No. 109801.
(11) Shakeri, M.; Shirzadeh Zarnagh, A. Crystallization of as-Mesocellular Silica Foam into Hierarchical TS-1 Zeolites by Conventional Hydrothermal and Dense-Gel Routes for Oxidation Reactions. *ACS Omega* **2020**, *5*, 9334−9338.
(12) Dong, J.; Zhu, H.; Xiang, Y.; Wang, Y.; An, P.; Gong, Y.; Liang, Y.; Qiu, L.; Zheng, A.; Peng, X.; et al. Toward a Unified Identification of Ti Location in the MFI Framework of High-Ti-Loaded TS-1: Combined EXAFS, XANES, and DFT Study. *J. Phys. Chem. C* **2016**, *120*, 20114−20124.
(13) Wu, L.; Deng, X.; Zhao, S.; Yin, H.; Zhuo, Z.; Fang, X.; Liu, Y.; He, M. Synthesis of a highly active oxidation catalyst with improved distribution of titanium coordination states. *Chem. Commun.* **2016**, *52*, 8679−8682.
(14) Chu, Q.; He, G.; Xi, Y.; Wang, P.; Yu, H.; Liu, R.; Zhu, H. Green synthesis of low-carbon chain nitroalkanes via a novel tandem reaction of ketones catalyzed by TS-1. *Catal. Commun.* **2018**, *108*, 46−50.
(15) Shen, X.; Wang, J.; Liu, M.; Li, M.; Lu, J. Preparation of the Hierarchical Ti-Rich TS-1 via TritonX-100-Assisted Synthetic Strategy for the Direct Oxidation of Benzene. *Catal. Lett.* **2019**, *149*, 2586−2596.
(16) Zuo, Y.; Liu, M.; Ma, M.; Song, C.; Guo, X. Improved Catalytic Performance for 1-Butene Epoxidation over Titanium Silicalite-1

Extrudates by Using SBA-15 or Carborundum as Additives. *Ind. Eng. Chem. Res.* **2017**, *56*, 7462−7467.
(17) Li, T.; Zuo, Y.; Guo, Y.; Yang, H.; Liu, M.; Guo, X. Highly stable TS-1 extrudates for 1-butene epoxidation through improving the heat conductivity. *Catal. Sci. Technol.* **2020**, *10*, 6152−6160.
(18) Wang, X.; Zhang, X.; Wang, Y.; Liu, H.; Wang, J.; Qiu, J.; Ho, H. L.; Han, W.; Yeung, K. L. Preparation and performance of TS-1/SiO_2 egg-shell catalysts. *Chem. Eng. J.* **2011**, *175*, 408−416.
(19) Wu, G.; Wang, Y.; Wang, L.; Feng, W.; Shi, H.; Lin, Y.; Zhang, T.; Jin, X.; Wang, S.; Wu, X.; et al. Epoxidation of propylene with H2O2 catalyzed by supported TS-1 catalyst in a fixed-bed reactor: Experiments and kinetics. *Chem. Eng. J.* **2013**, *215-216*, 306−314.
(20) Edwards, J. K.; Freakley, S. J.; Lewis, R. J.; Pritchard, J. C.; Hutchings, G. J. Advances in the direct synthesis of hydrogen peroxide from hydrogen and oxygen. *Catal. Today* **2015**, *248*, 3−9.
(21) Lin, M.; Xia, C.; Zhu, B.; Li, H.; Shu, X. Green and efficient epoxidation of propylene with hydrogen peroxide (HPPO process) catalyzed by hollow TS-1 zeolite: A 1.0kt/a pilot-scale study. *Chem. Eng. J.* **2016**, *295*, 370−375.
(22) Louis, B.; Reuse, P.; Kiwi-Minsker, L.; Renken, A. Synthesis of ZSM-5 coatings on stainless steel grids and their catalytic performance for partial oxidation of benzene by N_2O. *Appl. Catal., A* **2001**, *210*, 103−109.
(23) Shan, Z.; van Kooten, W. E. J.; Oudshoorn, O. L.; Jansen, J. C.; van Bekkum, H.; van den Bleek, C. M.; Calis, H. P. A. Optimization of the preparation of binderless ZSM-5 coatings on stainless steel monoliths by in situ hydrothermal synthesis. *Microporous Mesoporous Mater.* **2000**, *34*, 81−91.
(24) Li, Y.; Zhu, G.; Wang, Y.; Chai, Y.; Liu, C. Preparation, mechanism and applications of oriented MFI zeolite membranes: A review. *Microporous Mesoporous Mater.* **2021**, *312*, No. 110790.
(25) Wu, J.; Meng, X.; Chu, R.; Yu, S.; Wan, Y.; Song, C.; Zhang, G.; Zhao, T. Molecular dynamics simulation of the implantation of b-oriented ZSM-5 film modified α-quartz substrate surface with different modifiers. *Front. Chem.* **2019**, *7*, 746.
(26) Wu, A.; Tang, C.; Zhong, S.; Wang, B.; Zhou, J.; Zhou, R. Synthesis optimization of (h0h)-oriented silicalite-1 membranes for butane isomer separation. *Sep. Purif. Technol.* **2019**, *214*, 51−60.
(27) Ueno, K.; Negishi, H.; Okuno, T.; Tawarayama, H.; Ishikawa, S.; Miyamoto, M.; Uemiya, S.; Oumi, Y. Effects of Silica-Particle Coating on a Silica Support for the Fabrication of High-Performance Silicalite-1 Membranes by Gel-Free Steam-Assisted Conversion. *Membranes* **2019**, *9*, 46.
(28) Ueno, K.; Negishi, H.; Okuno, T.; Tawarayama, H.; Ishikawa, S.; Miyamoto, M.; Uemiya, S.; Oumi, Y. Effects of seed crystal type on the growth and microstructures of silicalite-1 membranes on tubular silica supports via gel-free steam-assisted conversion. *Microporous Mesoporous Mater.* **2019**, *289*, No. 109645.
(29) Kida, K.; Maeta, Y.; Yogo, K. Preparation and gas permeation properties on pure silica CHA-type zeolite membranes. *J. Membr. Sci.* **2017**, *522*, 363−370.
(30) Wang, X.; Meng, B.; Tan, X.; Zhang, X.; Zhuang, S.; Liu, L. Direct Hydroxylation of Benzene to Phenol Using Palladium−Titanium Silicalite Zeolite Bifunctional Membrane Reactors. *Ind. Eng. Chem. Res.* **2014**, *53*, 5636−5645.
(31) Chen, X.; Chen, P.; Kita, H. Pervaporation through TS-1 membrane. *Microporous Mesoporous Mater.* **2008**, *115*, 164−169.
(32) Li, Y.; Zhu, G.; Wang, Y.; Chai, Y.; Liu, C.; He, S. Effects of Substrate Surface Properties and Precursor Chemical Environment on InHsitu Oriented Construction of Titanium Silicalite Zeolite Membranes. *Gaodeng Xuexiao Huaxue Xuebao* **2021**, *42*, 2934−2943.
(33) Li, Y.; Zhu, G.; Wang, Y.; Chai, Y.; Liu, C.; He, S. In situ construction of an immobilized b-oriented titanium silicalite spherical molecular sieve membrane. *Appl. Surf. Sci.* **2021**, *563*, No. 150275.
(34) Qiu, F.; Wang, X.; Zhang, X.; Liu, H.; Liu, S.; Yeung, K. L. Preparation and properties of TS-1 zeolite and film using Sil-1 nanoparticles as seeds. *Chem. Eng. J.* **2009**, *147*, 316−322.
(35) Aguado, S.; Gascón, J.; Jansen, J. C.; Kapteijn, F. Continuous synthesis of NaA zeolite membranes. *Microporous Mesoporous Mater.* **2009**, *120*, 170−176.
(36) Dong, D.; Liu, B.; Chai, Y.; Wu, Y.; Liu, C. Dynamic hydrothermal synthesis of Silicalite-1 zeolite membrane to encapsulate defective porous alumina spheres Silicalite-1 Al_2O_3. *Chem. Ind. Eng. Prog.* **2018**, *37*, 3943−3948.
(37) Li, X.; Wang, Z.; Zheng, J.; Shao, S.; Wang, Y.; Yan, Y. Dynamic Hydrothermal Synthesis of a b-Oriented MFI Zeolite Film. *Chin. J. Catal.* **2011**, *32*, 217−223.
(38) Rao, K. T.; Mohan, Y. V.; Naveen; Rao, L. V. Estimation of H_2O_2 Content in Free Radical Bromination and Oxidation Reactions by the H_2O_2-HBr System Generated Effluent Samples by Iodometry Method. *Asian J. Chem.* **2013**, *25*, 4107−4108.
(39) Bordiga, S.; Damin, A.; Bonino, F.; Zecchina, A.; Spanò, G.; Rivetti, F.; Bolis, V.; Prestipino, C.; Lamberti, C. Effect of Interaction with H_2O and NH_3 on the Vibrational, Electronic, and Energetic Peculiarities of Ti(IV) Centers TS-1 Catalysts: A Spectroscopic and Computational Study. *J. Phys. Chem. B* **2002**, *106*, 9892−9905.
(40) Warren, B. *X-ray Diffraction*; Dover Publications, 1990.
(41) Tanabe, K. Surface and catalytic properties of ZrO_2. *Mater. Chem. Phys.* **1985**, *13*, 347−364.
(42) Boccuti, M. R.; Rao, K. M.; Zecchina, A.; Leofanti, G.; Petrini, G. Spectroscopic Characterization of Silicalite and Titanium-Silicalite. *Stud. Surf. Sci. Catal.* **1989**, *48*, 133−144.
(43) Notari, B. Synthesis and Catalytic Properties of Titanium Containing Zeolites. *Stud. Surf. Sci. Catal.* **1988**, *37*, 413−425.
(44) Vayssilov, G. N. Structural and physicochemical features of titanium silicalites. *Catal. Rev.: Sci. Eng.* **1997**, *39*, 209−251.
(45) Deka, R. C.; Nasluzov, V. A.; Ivanova Shor, E. A.; Shor, A. M.; Vayssilov, G. N.; Rösch, N. Comparison of All Sites for Ti Substitution in Zeolite TS-1 by an Accurate Embedded-Cluster Method. *J. Phys. Chem. B* **2005**, *109*, 24304−24310.
(46) van der Pol, A. J. H. P.; van Hooff, J. H. C. Parameters affecting the synthesis of titanium silicalite 1. *Appl. Catal., A* **1992**, *92*, 93−111.
(47) Duprey, E.; Beaunier, P.; Springuel-Huet, M. A.; Bozon-Verduraz, F.; Fraissard, J.; Manoli, J. M.; Brégeault, J. M. Characterization of Catalysts Based on Titanium Silicalite, TS-1, by Physicochemical Techniques. *J. Catal.* **1997**, *165*, 22−32.
(48) Uguina, M. A.; Serrano, D. P.; Ovejero, G.; Van Grieken, R.; Camacho, M. Preparation of TS-1 by wetness impregnation of amorphous SiO_2—TiO_2 solids: influence of the synthesis variables. *Appl. Catal., A* **1995**, *124*, 391−408.
(49) Guo, Q.; Sun, K.; Feng, Z.; Li, G.; Guo, M.; Fan, F.; Li, C. *A Thorough Investigation of the Active Titanium Species in TS-1 Zeolite by In Situ UV Resonance Raman Spectroscopy*. 2012, *18* (43), 13854−13860. DOI: 10.1002/chem.201201319.
(50) Li, C.; Xiong, G.; Liu, J.; Ying, P.; Xin, Q.; Feng, Z. Identifying Framework Titanium in TS-1 Zeolite by UV Resonance Raman Spectroscopy. *J. Phys. Chem. B* **2001**, *105*, 2993−2997.
(51) Koegler, J. H.; van Bekkum, H.; Jansen, J. C. Growth model of oriented crystals of zeolite Si-ZSM-5. *Zeolites* **1997**, *19*, 262−269.
(52) Meng, F.; Fan, Z.; Wu, Q.; Zhang, J.; Zhang, C.; Yang, Z.; Zhang, Y. Synthesis and Characterization of NaA Zeolite Membranes on the Inner Side of Hollow Fiber Support by a Dynamic Hydrothermal Process. *Mater. Rep.* **2017**, *31*, 168−172.
(53) Liu, X.; Wang, X.; Guo, X.; Li, G. Effect of solvent on the propylene epoxidation over TS-1 catalyst. *Catal. Today* **2004**, *93-95*, 505−509.

https://doi.org/10.1021/acsomega.3c02538
ACS Omega 2023, 8, 19099−19108